Available online at www.sciencedirect.com
ScienceDirect
Trans. Nonferrous Met. Soc. China 24(2014) 3293−3301

Transactions of Nonferrous Metals Society of China
www.tnmsc.cn

Numerical studies of effect of tool sizes and pin shapes on friction stir welding of AA2024-T3 alloy

Zhao ZHANG, Qi WU, Hong-wu ZHANG

State Key Laboratory of Structural Analysis for Industrial Equipment, Department of Engineering Mechanics, Faculty of Vehicle Engineering and Mechanics, Dalian University of Technology, Dalian 116024, China

Received 8 October 2013; accepted 6 January 2014

Abstract: Coupled thermo-mechanical model was used to investigate the effects of the pin diameter, the shoulder diameter and the in conical angle on the heat generations, the material deformations and the energy histories in friction stir welding (FSW) of AA2024-T3 alloy. Results indicate that the shoulder−plate contact area takes more important contribution to the heat generation than the pin-plate contact area. The increase of the shoulder diameter or the decrease of the pin diameter can lead to the increase of the welding temperature in FSW, but the change of shoulder size is more important. Compared to the cases in FSW of AA6061-T6, the input power is obviously increased in FSW of AA2024-T3 and the ratio of the plastic dissipation to the friction dissipation becomes decreased.

Key words: aluminum alloy; friction stir welding; coupled thermo-mechanical model; heat generation; energy history

1 Introduction

As a solid state joining technique, FSW shows advantages in joining thin plates of hard-to-weld materials [1]. FSW has been applied for the joining of aluminum alloys [2], magnesium alloys [3], titanium alloys [4], coppers [5], steels [6] and even dissimilar metals [7]. In FSW, a rotating tool is inserted into the butt of the joints. With the rotation of the tool, the material can be heated and then stirred. The material besides of the welding line can be mixed and then joined tightly by recrystallization.

The heat generation is very important for the forming of the tight joint in FSW and includes two parts: the heat generated by friction and the heat by plastic deformation [8]. More than 85% total efficient energy entering into the welding plate can be converted to heat by friction [9]. Compared to the frictional heat, the heat contribution from plastic deformation is smaller. Different models have been developed for the investigations on heat generations in FSW, including Eulerian model [10], ALE model [11], adaptive re-meshing model [12], moving heat source model [13], etc. In ALE model, the mesh movement in tangential direction is fixed to avoid mesh entanglements. The motions and maps of the mesh and the material play key role in the ALE simulation. Using the transformation of coordinates, the material coordinates can be easily described in each time step to trace the motion of the material particles. In adaptive re-meshing model, a fraction is selected for the program to conduct a check on each surface edge that has a contact node on each end. If the ratio exceeds the magnitude of the specified value, re-meshing will be triggered to avoid excessive mesh distortions in FSW processes. As stated by DAVID and DEBROY [14], the modeling of heat transfer, fluid flow and mass transfer can provide detailed insight into the welding processes. The material flows and heat transfers can be studied by the above mentioned numerical models. The direct material flow patterns can be further revealed by ALE model [15].

The material flows and the heat generations can be affected by the welding parameters and tool shapes in FSW [16]. Based on the principle of maximum utilization of supplied torque for traction, ARORA et

Foundation item: Project (NCET-12-0075) supported by the Program for New Century Excellent Talents in University, China; Project supported by the Fundamental Research Funds for the Central Universities, China; Projects (11172057, 11232003) supported by the National Natural Science Foundation of China; Project (2011CB013401) supported by the National Basic Research Program of China; Project (2012AA050901) supported by the National High-Tech Research and Development Program of China
Corresponding author: Zhao ZHANG; Tel/Fax: +86-411-84707608; E-mail: zhangz@dlut.edu.cn
DOI: 10.1016/S1003-6326(14)63469-5

al [17] proposed a criterion for the design of a tool shoulder diameter in FSW. BISWAS and MANDAL [18] studied the thermal histories in different tool geometries and different welding parameters in FSW.

Although many useful conclusions have been achieved in the investigations on the mechanism of FSW, the detailed relations between the energy inputs and the tool geometries have not been deeply studied. The investigations on the energy evolutions and the related heat generations can be useful for the tool design in FSW and for the further knowledge on the FSW mechanism. So, a fully coupled thermo-mechanical model based on solid mechanics is used to study the effects of the pin shapes and tool sizes on the heat generations and energy inputs in the FSW process of AA2024-T3.

2 Model description

A fully coupled thermo-mechanical model based on solid mechanics is used in current work. Arbitrary Lagrangian Eulerian (ALE) method is used to control the mesh distortions due to the movement of the welding tool. The success of this model in prediction of the welding temperature and the material deformation has been validated in Ref. [19]. Cylindrical and conical pins are used as shown in Fig. 1. The tool is treated as a rigid body in the simulation and the density is set to be 7850 kg/m^3. The welding parameters and the tool sizes are listed in Table 1. The thickness of the welding plate is 3 mm. The material of the plate is AA2024-T3. The mechanical and physical properties are listed in Ref. [8]. The dwelling time of 2 s and the axial load of 70 MPa are used.

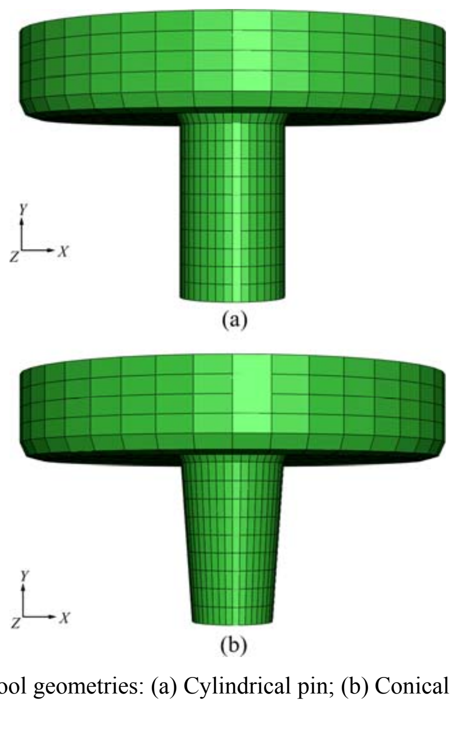

Fig. 1 Tool geometries: (a) Cylindrical pin; (b) Conical pin

Table 1 Welding parameters and tool sizes

Case	Shoulder diameter/ mm	Pin diameter/ mm	Conical angle/ (°)	Transverse speed/ (mm·s^{-1})	Rotating speed/ (r·min^{-1})
1	24	4	0	2.0	400
2	24	12	0	2.0	400
3	24	16	0	2.0	400
4	24	6	0	2.4	500
5	16	6	0	2.4	500
6	24	6	2	2.4	500
7	24	6	4	2.4	500

In FSW, the external work E_W can be converted to the kinematic energy, internal energy and frictional energy in FSW.

$$E_W = \int_0^t \iint_S \tau \cdot \dot{\gamma} \, \mathrm{d}S\mathrm{d}t + \iiint_V \frac{1}{2}\rho \boldsymbol{v} \cdot \boldsymbol{v} \mathrm{d}V + \left(\int_0^t \left(\int_V \sigma_v : \dot{\varepsilon} \mathrm{d}V\right) \mathrm{d}\tau + \int_0^t \left(\int_V \sigma_c : \dot{\varepsilon} \mathrm{d}V\right) \mathrm{d}\tau \right) \tag{1}$$

where σ_c is stress without viscous dissipation effect; σ_y is viscous stress; $\dot{\varepsilon}$ is strain rate; $\boldsymbol{v}$ is velocity vector; τ is frictional stress; $\dot{\gamma}$ is slipping rate; t is time; ρ is density; S is contact surface; V is volume.

Modified Coulomb friction law is more accurate for the description of the contact behavior on the tool-plate interface in FSW,

$$\tau_{\mathrm{crit}} = \min\left(\mu p, \frac{\sigma_s(T)}{\sqrt{3}} \right) \tag{2}$$

where μ is frictional coefficient; p is contact pressure; $\sigma_s(T)$ is yield stress at current temperature.

The slipping rate can be obtained from the velocity differences on the welding tool and the welding plate on the contact surfaces,

$$\dot{\gamma} = (v_{\mathrm{tool}} - v_{\mathrm{material}}) = \delta r \omega = \frac{2\pi n \delta r}{60} \tag{3}$$

where v_{tool} is linear velocity on tool surface; v_{material} is flow velocity on welding plate; δ is slipping factor; n is rotating speed, r/min; ω is rotating speed, rad/s; r is radial coordinate.

In each time increment, the dynamic motion equation and the heat transfer equation are solved,

$$\boldsymbol{M}\ddot{u} + \boldsymbol{C}\dot{u} + \boldsymbol{K}u = \boldsymbol{P} \tag{4}$$

$$\boldsymbol{C}_T \dot{T} + \boldsymbol{K}_T T = \boldsymbol{P}_T \tag{5}$$

where $\boldsymbol{M}$ is mass matrix; $\boldsymbol{C}$ is damping matrix; $\boldsymbol{K}$ is stiffness matrix; $\boldsymbol{P}$ is load vector; $\boldsymbol{C}_T$ is lumped capacitance matrix; $\boldsymbol{K}_T$ is heat transfer matrix; $\boldsymbol{P}_T$ is thermal load vector; u, $\dot{u}$ and $\ddot{u}$ are displacement, velocity and acceleration, respectively; T is temperature.

The mechanical solution response is obtained by using the explicit central-difference integration rule:

$$\dot{u}^N_{(i+\frac{1}{2})} = \dot{u}^N_{(i-\frac{1}{2})} + \frac{\Delta t_{(i+1)} + \Delta t_{(i)}}{2} \ddot{u}^N_{(i)} \tag{6}$$

where N is node number; i is increment number in an explicit dynamic step.

The central-difference integration operator is explicit due to the fact that the kinematic state is advanced using known values of $\dot{u}^N_{(i-\frac{1}{2})}$ and $\ddot{u}^N_{(i)}$ from the previous increment.

The heat transfer equations are integrated using the explicit forward-difference time integration rule:

$$T^N_{(i+1)} = T^N_{(i)} + \Delta t_{(i+1)} \dot{T}^N_{(i)} \tag{7}$$

The current temperature is obtained by using the known values from the previous increment. The values of $\dot{T}^N_{(i)}$ are computed at the beginning of the increment by

$$\dot{T}^N_{(i)} = \boldsymbol{C}^{-1}(\boldsymbol{P}^J_{(i)} - \boldsymbol{F}^J_{(i)}) \tag{8}$$

where $\boldsymbol{P}^J_{(i)}$ is the applied nodal source vector; $\boldsymbol{F}^J_{(i)}$ is the internal heat flux vector at the current increment.

Since both the forward-difference and the central-difference integrations are explicit, the heat transfer and mechanical solutions are obtained simultaneously by an explicit coupling. Error-corrector method can be used for the integration of the constitutive model [20]. The equivalent plastic strain $\bar{\varepsilon}^{\mathrm{p}}$ can be then obtained by the integration of strain rate $\dot{\varepsilon}^{\mathrm{p}}$.

$$\bar{\varepsilon}^{\mathrm{p}} = \int_0^t \sqrt{\frac{2}{3} \dot{\boldsymbol{\varepsilon}}^{\mathrm{p}} : \dot{\boldsymbol{\varepsilon}}^{\mathrm{p}}}\, \mathrm{d}t \tag{9}$$

The general finite element package ABAQUS with compiled FORTRAN code is used for the implementation of the above mentioned model.

3 Results and discussion

3.1 Effect of pin diameters

Two different pin diameters (Cases 1 and 2 listed in Table 1) are selected for comparison in temperature distributions around the welding tool, as shown in Fig. 2. When the pin diameter is 4 mm, the maximum welding temperature is 426.5 °C. When the pin diameter is increased to 12 mm, the maximum welding temperature is decreased to 419.6 °C. It is seen that the maximum welding temperature decreased with the increase of the pin diameters. With the increase of the pin diameter, the shoulder−plate contact area is decreased and the pin-plate contact area is increased. When the contact area between shoulder and plate is decreased by 22.9%, the maximum welding temperature is decreased by 1.62% although the pin-plate contact area is increased by 3 times simultaneously. This means that the shoulder−plate contact area is much more important than the pin-plate contact area in the heat generations in FSW.

The equivalent plastic strains defined in Eq. (9) in different pin diameters are shown in Fig. 3. When the pin diameter is 4 mm, the maximum equivalent plastic strain is 160.80. When the pin diameter is increased to 12 mm, the maximum equivalent plastic strain is decreased to 112.90. When the pin diameter is further increased to 16 mm (Case 3 in Table 1), the FSW fails to be simulated due to the occurrence of weld flaw. The maximum equivalent plastic strain is decreased with the increase of the pin diameter.

The energy histories including the external work, the frictional dissipated energy and the plastic dissipated energy in different pin diameters are shown in Fig. 4. When the pin diameter is 4 mm, the external work at 12 s

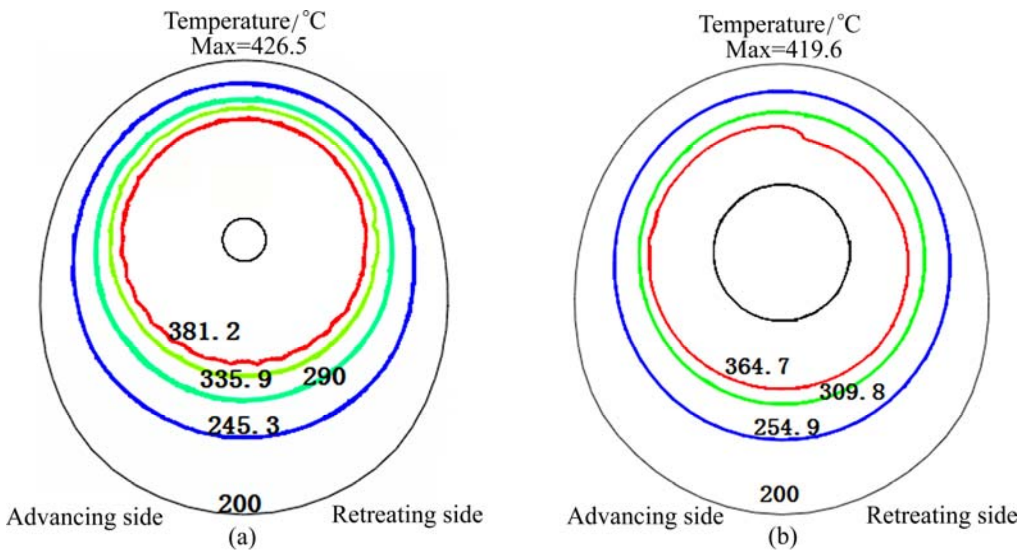

Fig. 2 Temperatures around welding tools with different pin diameters: (a) 4 mm; (b) 12 mm

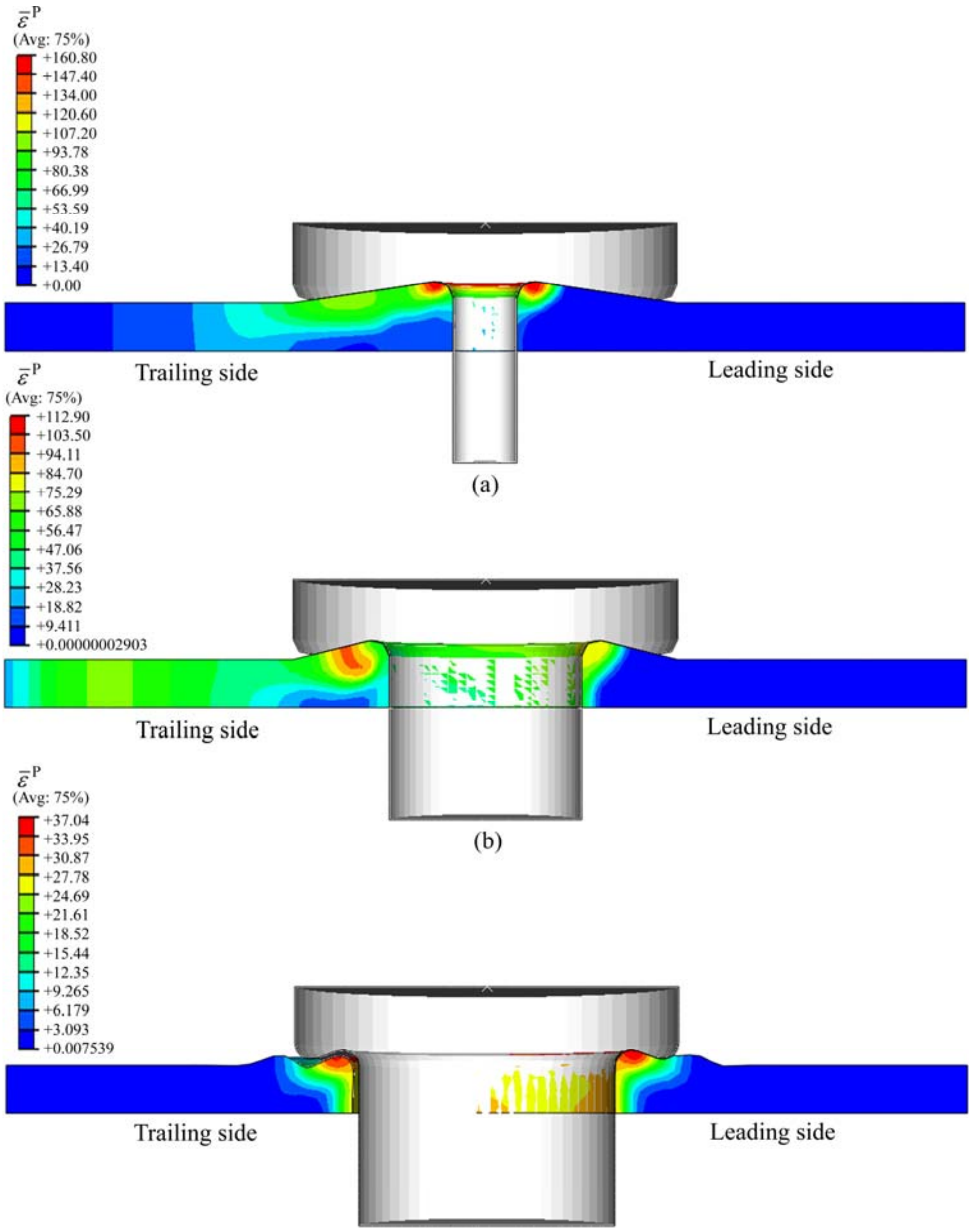

Fig. 3 Equivalent plastic strains around welding tools with different pin diameters: (a) 4 mm; (b) 12 mm; (c) 16 mm

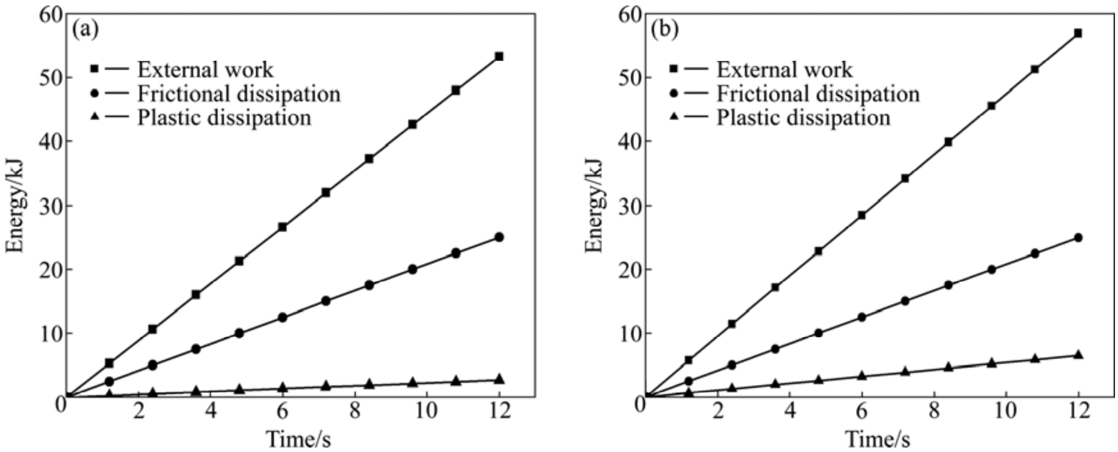

Fig. 4 Energy histories at different pin diameters: (a) 4 mm; (b) 12 mm

is 53.31 kJ. This means that the input power needed for FSW in current case is 4.44 kW. The frictional dissipation and the plastic dissipation are 25.03 kJ and 2.74 kJ, respectively. This means that the frictional and the plastic dissipation powers are 2.09 kW and 0.23 kW, respectively. When the pin diameter is increased to 12 mm, the input power is increased to 4.75 kW. The frictional and the plastic dissipation powers are 2.08 kW and 0.54 kW, respectively. Due to the decrease of the shoulder−plate contact area (22.9%) and the increase of the pin-plate contact area (3 times), the frictional dissipation is decreased. This means that the shoulder−plate contact surface takes the main contribution to the frictional dissipations in FSW with comparison to the pin-plate contact surface. Due to the fact that the frictional dissipation is higher than the plastic dissipation, it can be concluded that the shoulder−plate contact surface is the main factor for the heat generations in FSW. With the increase of the pin diameter, the plastic dissipated energy to heat is increased.

Compared to the cases in FSW of AA6061-T6 [15], the input power is obviously increased from 1.67 kW in FSW of AA6061 to 4.44 kW in FSW of AA2024 when the angular velocity is 400 r/min. AA2024-T3 shows higher yield stresses at lower temperature with comparison to AA6061-T6. In FSW, the material around the tool is heated and then stirred by the tool to form the tight weld on the trailing side. Higher input energy is needed to heat the material around the tool for the material with higher yield stresses to maintain the flowability. This may be the reason for the increase of the input power for the case in FSW of AA2024. The ratio of the plastic dissipation to the friction dissipation becomes decreased in FSW of AA2024-T3. This means that the plastic dissipated energy takes more important contribution in FSW of AA6061-T6 with comparison to the FSW of AA2024-T3.

3.2 Effect of shoulder diameter

Two cases of different shoulder diameters are compared (Cases 4 and 5 in Table 1). When the shoulder diameters are 24 mm and 16 mm, the maximum welding temperatures are 429.4 °C and 351.2 °C, respectively, as shown in Fig. 5. The maximum welding temperature is decreased by 18.2% when the shoulder−plate contact area is decreased by 55.6%. When the shoulder diameter is decreased, it can be also seen that the temperature under the shoulder becomes un-uniform. The temperature in the rear half of the shoulder becomes higher than the front side.

The maximum equivalent plastic strain is decreased from 161.10 to 131.50 when the shoulder diameter is decreased, as shown in Fig. 6. The material deformation is increased with the increase of the shoulder diameter.

The energy variations with time at different shoulder diameters are shown in Fig. 7. The external work, the frictional dissipation and the plastic dissipation are 55.42, 25.77 and 3.19 kJ at 11.5 s when the shoulder diameter is 24 mm, respectively. The input power, the frictional dissipation power and the plastic dissipation power can then be calculated as 4.82, 2.24 and 0.28 kW, respectively. When the shoulder diameter is decreased to 16 mm, the external work, the frictional dissipation and the plastic dissipation are decreased to be 29.94, 13.21 and 3.15 kJ, and the corresponding powers are 2.6, 1.15 and 0.27 kW, respectively. When the shoulder−plate contact area is decreased by 55.6%, the input power is decreased by 46.1%. It can be seen that the variation of the shoulder diameter is more important than the variation of the pin diameter to the energy inputs needed for FSW. 52.3% of the total energy input can be

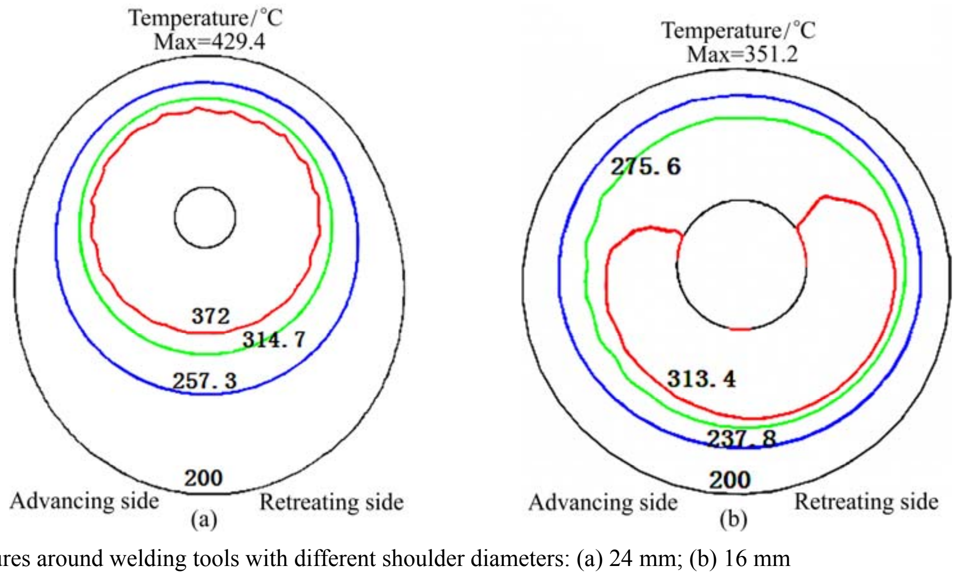

Fig. 5 Temperatures around welding tools with different shoulder diameters: (a) 24 mm; (b) 16 mm

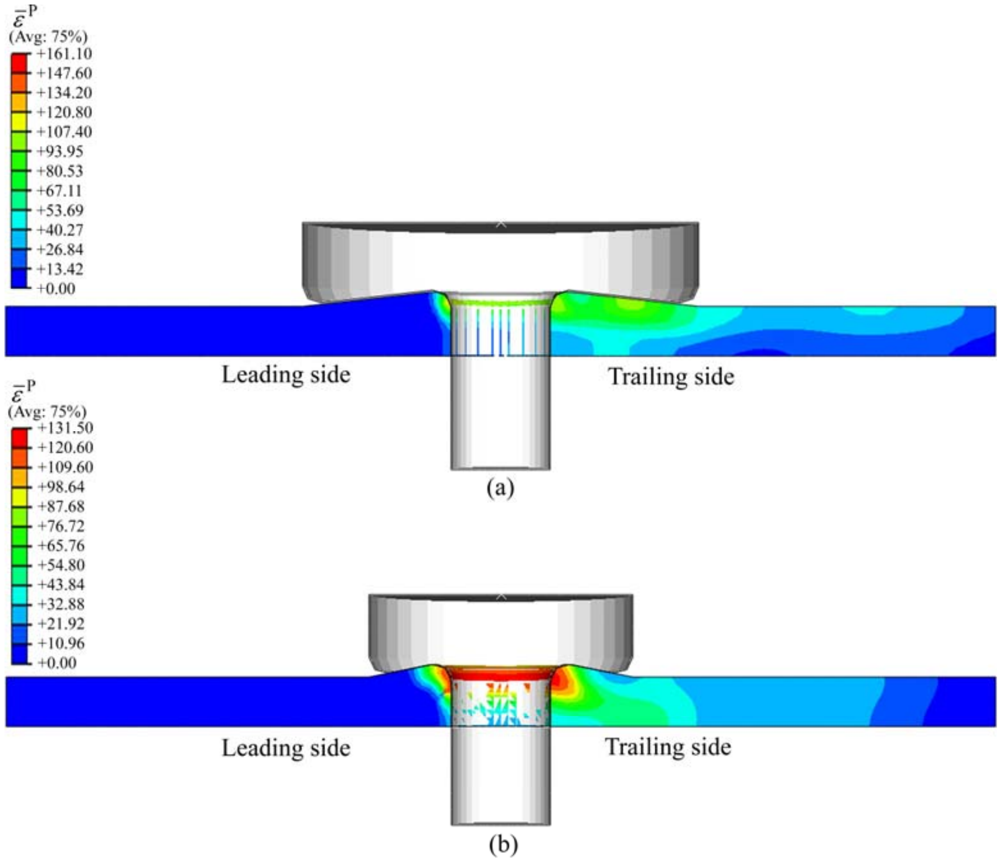

Fig. 6 Equivalent plastic strains around welding tools with different shoulder diameters: (a) 24 mm; (b) 16 mm

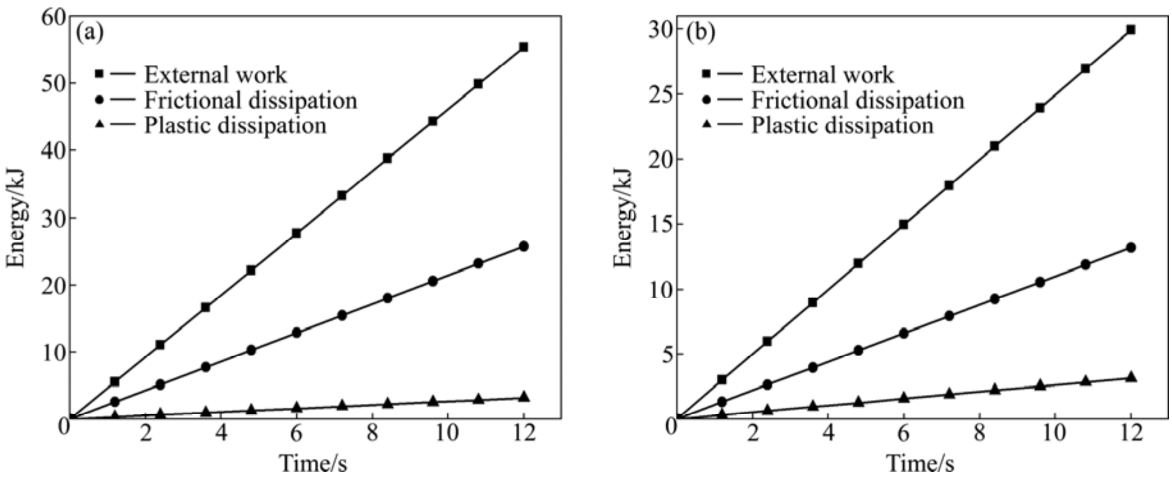

Fig. 7 Energy histories at different shoulder diameters: (a) 24 mm; (b) 16 mm

converted to heat when the shoulder diameter is 24 mm. This ratio is increased to be 54.6% when the shoulder diameter is decreased. The energy ratio converted to heat is increased with the decrease of the shoulder diameter.

3.3 Effect of conical angles

The temperature fields at different conical angles (Cases 6 and 7 in Table 1) are shown in Fig. 8. When the conical angle of the pin is 2°, the maximum temperature is 423.5 °C. When the conical angle is increased to 4°, the maximum welding temperature is increased to 425.7 °C. In the current two cases, the shoulder−plate contact area is the same. The slight increase of the pin-plate contact area leads to the increase of the temperature.

Figure 9 shows the distributions of the equivalent plastic strain in different conical angles. When the conical angle is increased from 2° to 4°, the maximum

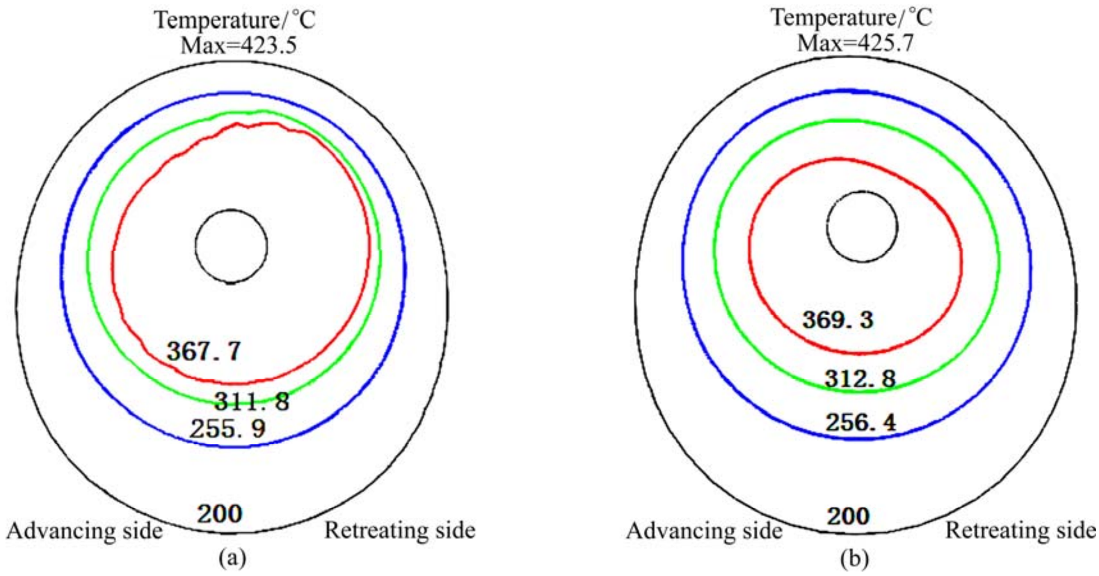

Fig. 8 Temperatures around welding tools with different conical angles: (a) 2°; (b) 4°

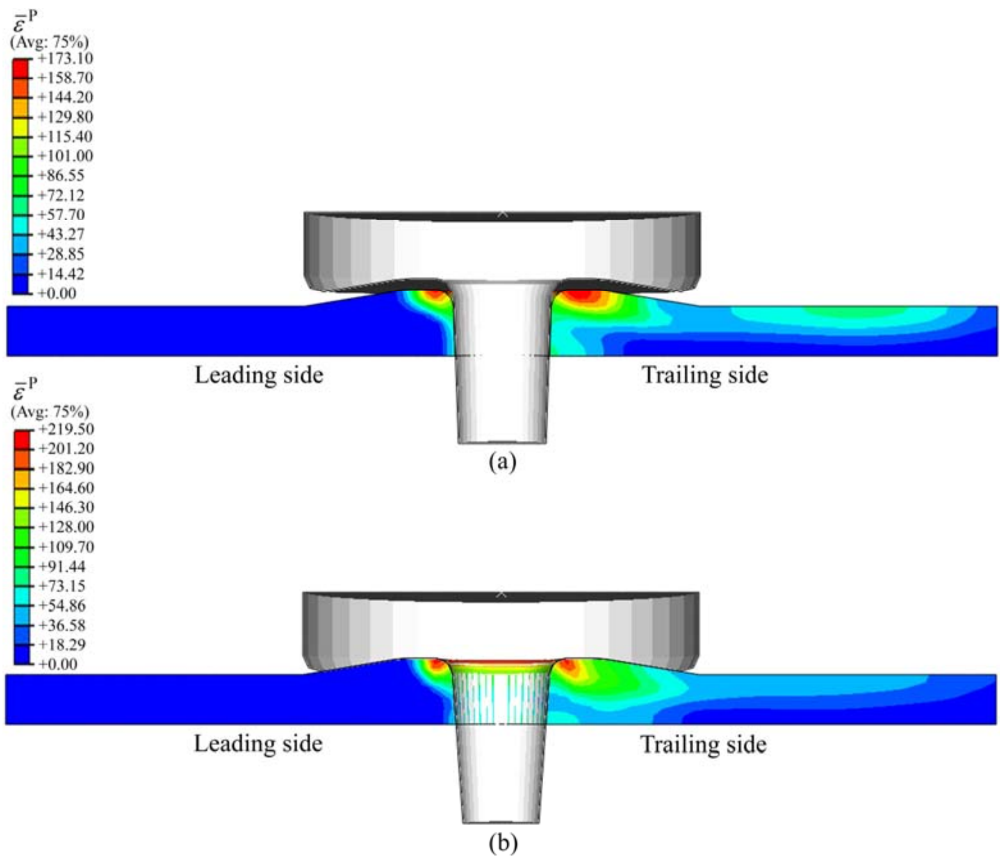

Fig. 9 Equivalent plastic strains around welding tools with different conical angles: (a) 2°; (b) 4°

equivalent plastic strain is increased from 173.10 to 219.5. This means that the increase of the conical angle can be useful for the improvement of the flowability of the material around the welding tool.

The energy variations with time at different conical angles are shown in Fig. 10. The input total energies in both the cases are very similar. The input power can be calculated from Fig. 10 to be 4.55 kW. The frictional dissipation energy is slightly increased from 2.08 kW to 2.09 kW when the conical angle is increased from 2° to 4°. The contact area including the pin-plate and the shoulder plate contact surfaces is very similar in both two cases. This is the reason for the similarity of the energies in current cases.

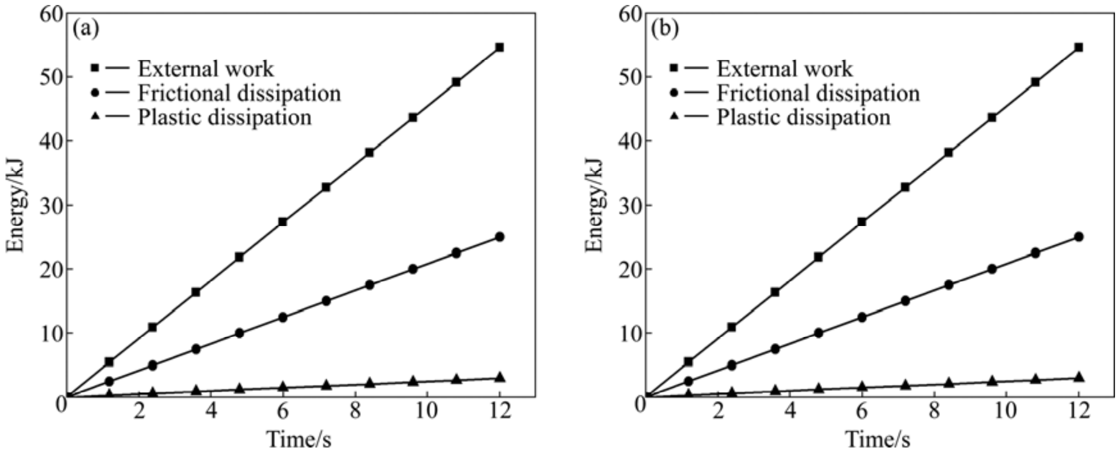

Fig. 10 Energy histories at different conical angles: (a) 2°; (b) 4°

4 Conclusions

1) The shoulder−plate contact surface takes the main contribution to the frictional dissipations in FSW. Due to the fact that the frictional dissipation is higher than the plastic dissipation, the shoulder−plate contact surface is the main factor for the heat generations in FSW.

2) Compared to the cases in FSW of AA6061-T6, the input power is obviously increased in FSW of AA2024-T3 and the ratio of the plastic dissipation to the friction dissipation becomes decreased.

3) When the shoulder−plate contact area is decreased by 55.6%, the input power is decreased by 46.1%. The variation of the shoulder diameter is more important to the energy inputs needed for FSW than the variation of the pin diameter.

4) The dissipated energy ratio into heat is increased with the decrease of the shoulder diameter. The energy ratio converted to heat is increased with the decrease of the shoulder diameter.

References

[1] MISHRA R S, MA Z Y. Friction stir welding and processing [J]. Materials Science and Engineering R, 2005, 50: 1−78.

[2] RAJAKUMAR S, MURALIDHARAN C, BALASUBRAMANIAN V. Establishing empirical relationships to predict grain size and tensile strength of friction stir welded AA6061-T6 aluminium alloy joints [J]. Transactions of Nonferrous Metals Society of China, 2010, 20: 1863−1872.

[3] ZHOU L, NAKATA K, LIAO J, TSUMURA T. Microstructural characteristics and mechanical properties of non-combustive Mg−9Al−Zn−Ca magnesium alloy friction stir welded joints [J]. Materials & Design, 2012, 42: 505−512.

[4] NANDAN R, LIENERT T J, DEBROY T. Toward reliable calculations of heat and plastic flow during friction stir welding of Ti−6Al−4V alloy [J]. International Journal of Materials Research, 2008, 99: 434−444.

[5] SAKTHIVEL T, MUKHOPADHYAY J. Microstructure and mechanical properties of friction stir welded copper [J]. Journal of Materials Science, 2007, 42: 8126−8129.

[6] BHADESHIA H K D H, DEBROY T. Critical assessment: Friction stir welding of steels [J]. Science and Technology of Welding and Joining, 2009, 14: 193−196.

[7] LEE W B, YEON Y M, JUNG S B. The mechanical properties related to the dominant microstructure in the weld zone of dissimilar formed Al alloy joints by friction stir welding [J]. Journal of Materials Science, 2003, 38: 4183−4191.

[8] ZHANG Z, CHEN J T, ZHANG Z W, ZHANG H W. Coupled thermo-mechanical model based comparison of friction stir welding processes of AA2024-T3 in different thicknesses [J]. Journal of Materials Science, 2011, 46: 5815−5821.

[9] ZHANG Z, CHEN J T. Computational investigations on reliable finite element-based thermomechanical-coupled simulations of friction stir welding [J]. International Journal of Advanced Manufacturing Technology, 2012, 60: 959−975.

[10] JACQUIN D, de MEESTER B, SIMAR A, DELOISON D, MONTHEILLET F, DESRAYAUD C. A simple Eulerian thermomechanical modeling of friction stir welding [J]. Journal of Materials Processing Technology, 2011, 211: 57−65.

[11] SCHMIDT H, HATTEL J. A local model for the thermomechanical conditions in friction stir welding [J]. Modelling and Simulation in Materials Science and Engineering, 2005, 13: 77−93.

[12] ASADI P, MAHDAVINEJAD R A, TUTUNCHILAR S. Simulation and experimental investigation of FSP of AZ91 magnesium alloy [J]. Materials Science and Engineering A, 2011, 528: 6469−6477.

[13] YAN D Y, WU A P, SILVANUS J, SHI Q Y. Predicting residual distortion of aluminum alloy stiffened sheet after friction stir welding by numerical simulation [J]. Materials & Design, 2011, 32: 2284−2291.

[14] DAVID S A, DEBROY T. Current issues and problems in welding sciences [J]. Science, 1992, 257: 497−502.

[15] ZHANG Z, ZHANG H W. Numerical studies on controlling of process parameters in friction stir welding [J]. Journal of Materials Processing Technology, 2009, 209: 241−270.

[16] KUMAR R, SINGH K, PANDEY S. Process forces and heat input as function of process parameters in AA5083 friction stir welds [J]. Transactions of Nonferrous Metals Society of China, 2012, 22: 288−298.

[17] ARORA A, de A, DEBROY T. Toward optimum friction stir welding shoulder diameter [J]. Scripta Materialia, 2011, 64: 9−12.
[18] BISWAS P, MANDAL N R. Effect of tool geometries on thermal history of FSW of AA1100 [J]. Welding Journal, 2011, 90(Suppl): 129−135.
[19] ZHANG Z, ZHANG H W. A fully coupled thermo-mechanical model of friction stir welding [J]. International Journal of Advanced Manufacturing Technology, 2008, 37: 279−293.
[20] ZHANG H W, ZHANG Z, BIE J, ZHOU L, CHEN J T. Effect of viscosity on material behaviors in friction stir welding process [J]. Transactions of Nonferrous Metals Society of China, 2006, 16: 1045−1052.

2024-T3 铝合金搅拌摩擦焊接中搅拌头尺寸和搅拌针形状影响的数值模拟

张 昭，吴 奇，张洪武

大连理工大学 工程力学系 工业装备结构分析国家重点实验室，大连 116024

摘 要：采用完全热力耦合模型研究了搅拌针直径、轴肩直径以及搅拌针锥角对 2024-T3 铝合金搅拌摩擦焊接过程中热生成、材料变形和能量历史的影响。结果表明：相比搅拌针接触面，轴肩接触面对搅拌摩擦焊接的热生成起主要作用。增加轴肩直径和减小搅拌针直径均能增加焊接温度，但是轴肩尺寸变化的影响更为明显。与 6061-T6 铝合金的搅拌摩擦焊接过程相比，2024-T3 铝合金搅拌摩擦焊接的能量输入明显增加，同时塑性耗散与摩擦耗散的能量比减小。

关键词：铝合金；搅拌摩擦焊；完全热力耦合模型；热生成；能量历史

(Edited by Yun-bin HE)